REPORT DOCUMENTATION PAGE

Form Approved
OMB No. 0704-0188

1. REPORT DATE *(DD-MM-YYYY)*	**2. REPORT TYPE**	**3. DATES COVERED** *(From - To)*
27 July 2016	Conference Paper	13 June 2016 – 27 July 2016

4. TITLE AND SUBTITLE
Large Eddy Simulations of Transverse Combustion Instability in a Multi-Element Injector

5a. CONTRACT NUMBER

5b. GRANT NUMBER

5c. PROGRAM ELEMENT NUMBER

6. AUTHOR(S)
M. Harvazinski, Y. Desai, D. Talley, V. Sankaran

5d. PROJECT NUMBER

5e. TASK NUMBER

5f. WORK UNIT NUMBER
Q0YA

7. PERFORMING ORGANIZATION NAME(S) AND ADDRESS(ES) AND ADDRESS(ES)

Air Force Research Laboratory (AFMC)
AFRL/RQRC
10 E. Saturn Blvd.
Edwards AFB, CA 93524-7680

8. PERFORMING ORGANIZATION REPORT NO.

9. SPONSORING / MONITORING AGENCY NAME(S) AND ADDRESS(ES)

Air Force Research Laboratory (AFMC)
AFRL/RQR
5 Pollux Drive
Edwards AFB, CA 93524-7048

10. SPONSOR/MONITOR'S ACRONYM(S)

11. SPONSOR/MONITOR'S REPORT NUMBER(S)
AFRL-RQ-ED-TP-2016-153

12. DISTRIBUTION / AVAILABILITY STATEMENT
Approved for Public Release; Distribution Unlimited. The U.S. Government is joint author of the work and has the right to use, modify, reproduce, release, perform, display, or disclose the work. PA Clearance Number: 16315 Clearance Date: 6/22/2016

13. SUPPLEMENTARY NOTES
For presentation at AIAA Propulsion and Energy 2016; Salt Lake City UT; July 25-27, 2016
Prepared in collaboration with HyPerComp, Inc.

14. ABSTRACT

Large Eddy Simulation (LES) is applied to study transverse combustion instability in a seven element combustor. The combustor is a self-excited linear array of seven elements. Different levels of instability are produced by changing which injectors flow fuel. Two configurations were analyzed, the most stable and the most unstable experimental configuration. The simulations showed different behavior for each case. For the unstable case, the simulated amplitudes were lower than the experimental, and there was not a well-defined transverse wave present in the combustor. Interestingly in this case the center element coupled with the first mode in the combustor and appeared to have a stabilizing effect. The amplitude of the simulated stable case was larger than the experimental, but showed evidence of a transverse instability.

15. SUBJECT TERMS
N/A

16. SECURITY CLASSIFICATION OF:			**17. LIMITATION OF ABSTRACT**	**18. NUMBER OF PAGES**	**19a. NAME OF RESPONSIBLE PERSON**
					D. Talley
a. REPORT	**b. ABSTRACT**	**c. THIS PAGE**	SAR	28	**19b. TELEPHONE NO** *(include area code)*
Unclassified	**Unclassified**	**Unclassified**			N/A

Standard Form 298 (Rev. 8-98)
Prescribed by ANSI Std. 239.18

Large Eddy Simulations of Transverse Combustion Instability in a Multi-Element Injector

Matthew E. Harvazinski*,
Air Force Research Laboratory, Edwards AFB, CA, 93524
Yogin Desai†,
HyPerComp, Inc., Westlake Village, CA, 91361
Douglas G. Talley‡, and Venkateswaran Sankaran§
Air Force Research Laboratory, Edwards AFB, CA, 93524

Large Eddy Simulation (LES) is applied to study transverse combustion instability in a seven element combustor. The combustor is a self-excited linear array of seven elements. Different levels of instability are produced by changing which injectors flow fuel. Two configurations were analyzed, the most stable and the most unstable experimental configuration. The simulations showed different behavior for each case. For the unstable case, the simulated amplitudes were lower than the experimental, and there was not a well-defined transverse wave present in the combustor. Interestingly in this case the center element coupled with the first mode in the combustor and appeared to have a stabilizing effect. The amplitude of the simulated stable case was larger than the experimental, but showed evidence of a transverse instability.

I. Introduction

Combustion instability has plagued the development of liquid rocket engines and remains a large risk in the development and acquisition of new liquid rocket engines. Combustion instability is the coupling between unsteady combustion and acoustics. Under the correct conditions a feedback loop is established which can allow for large amplitude pressure oscillations to take place in the engine. The amplitude of these oscillations can be of the same order of magnitude as the chamber pressure. In the most extreme cases this will result in a catastrophic failure of the engine. Under less severe conditions locally increased heat transfer can occur leading to damage as well as negative performance implications. While all combustion devices are susceptible to instability, rockets are particularly prone due to their high energy densities and acoustic compactness.[1] No truly predictive model exists. This is partly because changes to the operating conditions, propellants, or injector geometry all have the potential to modify the stability map of an engine. This makes the design process extremely difficult because simple correlations between design parameters and the stability map are not available. Often times the instability (or stability) is not identified until after the hardware is built. Eliminating an instability at this point can be expensive and time consuming, as was demonstrated in the development of the F-1 engine.[2]

Recently, high fidelity computational fluid dynamics (CFD) of reacting flow has been used to simulate sub-scale experiments. The efforts have focused on validating the potential use of CFD to study instability followed by the application of the simulations to better understand the physics that can lead combustion instability in liquid rocket engines. Simulations of this type are able to capture the relevant physics including mixing, combustion, acoustics, geometry, and their interactions.[3–10] Lower order approaches like wave equation based models use empirical models for key aspects of the physics, for example the combustion

*Research Aerospace Engineer, AIAA Member.
†Member of the Technical Staff, AIAA Member.
‡Research Physical Scientist, AIAA Associate Fellow.
§Senior Scientist, AIAA Senior Member.

source term.[11,12] This limits their applicability in new or novel designs, or in building a fundamental understanding of the instability. The conditions inside the combustor during an instability are highly unsteady and non-linear, which does not allow for investigations using inexpensive steady state Reynolds-Averaged based simulations. Instead, unsteady large eddy simulations (LES) or detached eddy simulations (DES) are required, often with considerable run times to obtain sufficient data for analysis. Typical single element simulations will require 1000s of cores for multiple weeks. The majority of modeling efforts has been focused on single element studies, partly due to the computational cost of these studies.

A large body of single element work has focused on the continuously varying resonance combustor (CVRC) from Purdue University.[13] Simulations by multiple groups have produced good agreement with experimental results. In the CVRC, the varying oxidizer post length yields different levels of instability amplitude. Both stable and unstable configurations have been accurately modeled. A comprehensive review of the computational work done on the CVRC was completed by Harvazinski et al.[10] In the CVRC the amplitude is controlled by the relative timing of the acoustic waves in the oxidizer post and combustor. In the unstable configuration these waves temporarily stop the fuel flow into the combustor producing a cyclic heat release that is in sync and couples with the acoustic waves. In the stable configuration there is continuous heat release because of the wave timings. The instability in the CVRC is longitudinal, whereas the most damaging of instabilities found in liquid rocket engines are transverse. The motivating of the experiment behind the current work is to subject the CVRC injector to transverse instability and understand how it behaves. A multi-element setup is used to produce the self-excited transverse instability.

II. Background

The present study is of the transverse instability combustor (TIC) from Purdue University.[14] The TIC is a multi-element test rig with 7 elements arranged in a linear array. The combustor is rectangular with a tapered converging nozzle affixed to the end. This represents the second iteration of the TIC, this version uses slightly different injectors and propellants compared with the first, but the overall arrangement and size of the injectors is the same.[15,16] Under driving conditions, a high amplitude transverse wave is established in the combustor which interacts with the injectors. A schematic of the experiment is shown in Figure 1. The oxidizer is decomposed hydrogen peroxide which is supplied through a manifold; a perforated plate separates the oxidizer manifold and the injectors, acoustically isolating the manifold from the injectors and the combustor. The center element, described as the study element, is similar to the CVRC injector. A series of co-annular choked slots are used to separate the oxidizer manifold and the injector instead of the perforated plate.

The fuel used in the study element is ethane (C_2H_6) and the driving elements use RP1. Four different levels of instability were demonstrated experimentally; this was done by varying which of the driving injectors flowed fuel. Each element always flowed oxidizer and the study element flowed both fuel and oxidizer. Four different injector configurations are tabulated in Table 1. Bi-propellant flow is represented by 'O' and oxidizer-only flow through the injector is represented by 'X'. Amplitudes ranged from 65% of the chamber pressure to 8% of the chamber pressure. The most unstable configuration was where the two outer elements on each side were flowing both fuel and oxidizer. The most stable configuration had three injectors that flowed both fuel and oxidizer compared with five in the most unstable case. Note that the level of observed instability is a function of both the number and locations of the driving injectors. For this study configurations 1 and 4 are examined.

Table 1: TIC configurations and observed amplitides, 'O' indicates bi-propellant flow, 'X' indicates oxidier only flow.[17]

No.	Configuration	p', $\%p_c$
1	OOXOXOO	65%
2	OXXOXXO	50%
3	XOOOOOX	20%
4	XOXOXOX	8%

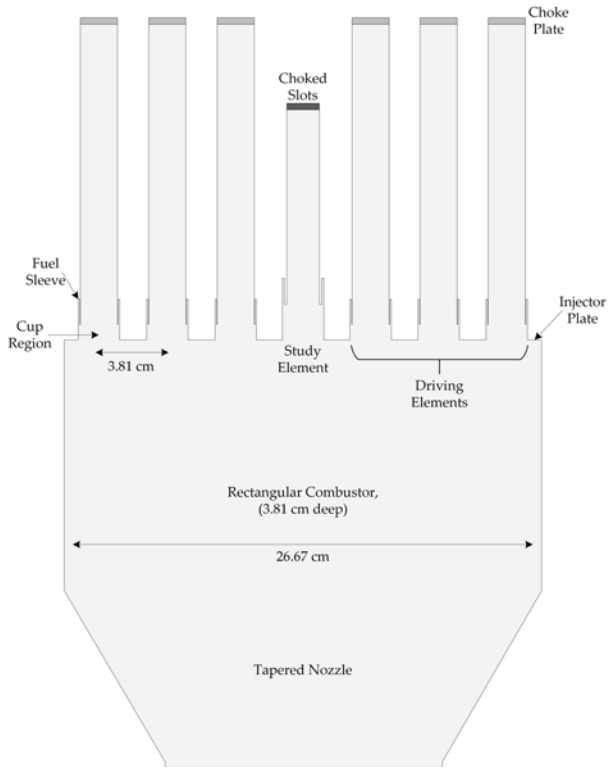

Figure 1: Sketch of the TIC.

Several prior studies have looked at modeling the TIC. The first by Morgan et al. used a reduced three injector model. The two outermost injectors on either side were replaced with a constant mass flow of warm combustion products. The transverse instability was established by artificially vibrating the side walls of the chamber. By tuning the wall boundary condition frequency and amplitude conditions were matched to the experimental values. This allowed for a detailed study of how the center study injector responded to a transverse instability.[17] Tudisco et al. investigated a later version of the TIC that used methane (CH_4) for the fuel, also using the reduced three injector approach with artificial forcing. The authors examined both forced and unforced cases. In both instances they found that a correlation between the heat release from the center injector and the acoustic waves in the chamber did not exist.[18] The limitation with this model is that the setup of the transverse instability is artificially forced, unlike the experiment which is self-excited. Shipley et al. further examined the TIC using a full simulation of all seven injectors. The experimental configuration modeled was the same that Tudisco et al. studied. Results from this work showed that vortex impingement from the driving injectors took place during the periods of high amplitude instability. There was impingement between injectors, and also between the injectors and the combustor walls. Unlike the experiment this simulation never reached a limit cycle. There was a long transient behavior which showed periods of instability growth and instability damping.[19]

The current C_2H_6/RP1 setup was also modeled using a reduced approach where the solution was solved on multiple coupled grids by Popov and Sirignano. In their approach one-dimensional grids are used inside the injector ports, two-dimensional axisymmetric grids are used to model the combustion region in the chamber and a two-dimensional planar grid is used for the acoustics in the combustor. They obtained excellent agreement with experimental results, under predicting the amplitude in each case by only 4-8%.[20] The limitation of this work is that it exploits the geometry of the current setup to make simplifications. This type of simplification is not likely to be available in actual engines which are circular and often feature asymmetric injector layouts.

III. Computational Model

A. Computational Domain and Test Conditions

The computational mesh of the test rig is shown in Figure 2. Decomposed hydrogen peroxide is used as oxidizer in all injectors. To limit the computational domain for simulation, some approximations were made to the geometry. In the experiments, a perforated choke plate is used to the choke oxidizer flow. In this study the choke plate is not included, instead a constant mass flow rate which is perfectly reflecting (to mimic the effect of the flow choking) is used. The choked slots in the study element are also replaced by a constant mass flow boundary. A previous study using the single injector element from the CVRC compared the choked slots with constant a mass flow inlet. The results showed that constant mass flow inlet appropriately captures the primary modes of the instability.[21] Similarly, the fuel injection system from the experiment is not modeled. The fuel is assumed to enter through a narrow annular slot. The computational mesh is a multi-block hexahedral mesh containing 15.63 million cells. For each injector, 14 cells are used to resolve fuel annulus and 56 cells are used to resolve oxidizer tube in the radial direction.

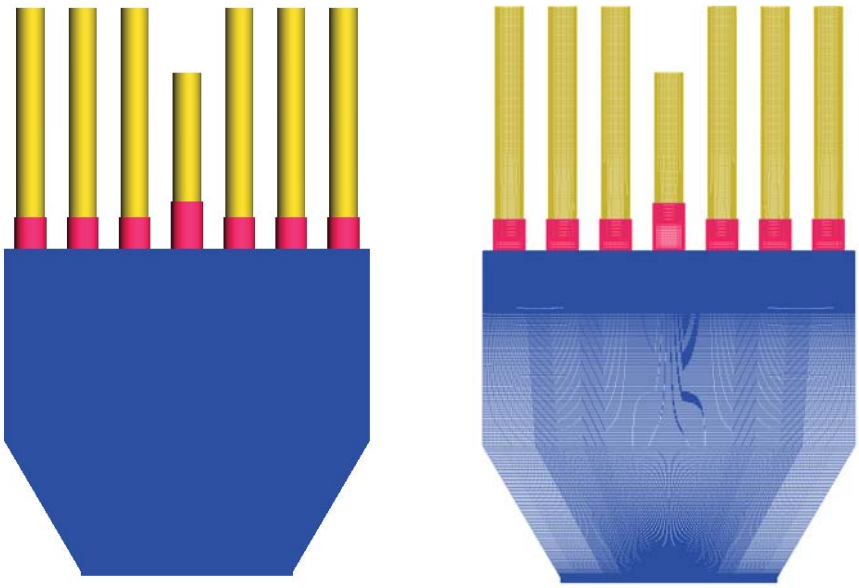

Figure 2: Model geometry (left) showing oxidizer tubes (in yellow) and fuel tubes (in Red). The computational Mesh is shown to the right and contains 15.63 million hexahedral cells.

B. Solver Formulation and Methodology

A mature reacting flow CFD code is used for the present work, the code used is LESLIE. LESLIE was developed by Menon et al and is a large eddy simulation code that is explicit in time and operates on multi-block structured grids. It is a second-order accurate (in both space and time) finite-volume formulation which solves the unsteady Favre-filtered multi-species compressible LES equations.[22,23] Regions of high gradients are accurately captured by using a hybrid scheme that switches between a second-order accurate central scheme and a third-order accurate MUSCL (Monotone Upstream-centered Schemes for Conservation Laws) scheme.[24] The hybrid scheme uses a localized dynamic switch[25,26] based on density and pressure gradients to determine local spatial discretization scheme. A sub-grid eddy-viscosity based model that utilizes the sub-grid kinetic energy (k^{sgs}) as characteristic velocity scale and a local filter size as characteristic length scale is used to close unclosed terms in the filtered momentum and energy equations.[24,27] A finite rate chemistry model is used to model reaction-diffusion terms. Further specific details on numerical formulation,

code implementation and validation can be found in Ref. 22-27.

C. Initial and Boundary Conditions

Decane ($C_{10}H_{22}$) is used as a single species surrogate for RP1 which is used in the driving elements. Decomposed hydrogen peroxide in the oxidizer inflow is modeled as a uniform mixture of 58% water and 42% oxygen (by mass). The inflow boundaries for fuel and oxidizer are modeled using constant mass boundary conditions with prescribed mass flow rates, temperature and species mass fractions. The inflow boundary conditions for the fuel and oxidizer ports are summarized described in Table 2. All walls in the combustor are modeled as adiabatic no-slip walls. The outlet of the combustor was modeled with mixed outflow boundary conditions where the local Mach number is used to switch between a subsonic and supersonic formulation. In the case of subsonic flow, the atmospheric pressure is supplied as the boundary condition. All species are modeled using the thermally perfect gas assumption with thermodynamic properties evaluated through polynomial curve-fit data. Power law relationships are used to obtain the transport properties of each species.

Table 2: Inflow boundary specifications.

Inlet	Mass flow rate, kg/s	Temperature, K	Species mass fractions
Oxidizer inlet	0.196	1029.0	H_2 0.58, O_2 0.42
Study element fuel	0.025	319.0	C_2H_6 1.0
Driving element fuel	0.033	298.15	$C_{10}H_{22}$ 1.0

Initially, the entire rectangular combustor chamber along with cup region is filled with products (48% CO_2 and 52% H_2O) at 2000 K. Fuel is initialized with inflow conditions in the annulus region from the fuel inlet up to the cup region. Similarly, decomposed hydrogen peroxide is initialized with inflow conditions in the oxidizer tube up to the cup region. The entire domain is initialized with a chamber pressure of 900 kPa. The higher temperature in the combustor cup ensures ignition when the fuel and oxidizer mix. Previous studies involving a similar initial condition strategy showed that the final pressure perturbation amplitude and frequency are insensitive to initial temperature as long as a flame is established.[4] For the current study, the flow through time was approximated to be 3 ms. The flow through time for the current geometry is based on the bulk velocity at the oxidizer inlet and total axial length of the domain. All simulations are run for 7 flow-through times (20 ms) to eliminate the transient start up effects.

D. Reaction Mechanism

A 4-step 6-species (C_2H_6, $C_{10}H_{22}$, O_2, CO_2, H_2O, and CO) global finite rate kinetics model is used to model combustion. The four reactions in the chemical mechanism are given below,[28]

$$C_2H_6 + 2.5\,O_2 \longrightarrow 2\,CO + 3\,H_2O \tag{1}$$
$$C_{10}H_{22} + 10.5\,O_2 \longrightarrow 10\,CO + 11\,H_2O \tag{2}$$
$$CO + 0.5\,O_2 \longrightarrow CO_2 \tag{3}$$
$$CO_2 \longrightarrow CO + 0.5\,O_2 \tag{4}$$

Although the global chemical mechanism does not model the effects of the intermediate species in the kinetics, the ability of the heat release to couple the pressure is the key requirements and global kinetics provide that. As a result, the above 4-step global mechanism is deemed sufficient for combustion modeling based on prior work.[10,29] The forward reaction rates for each chemical equation are given below,

$$k_{1,f} = 7.31 \times 10^9 e^{-15097/T} \left[C_2H_6\right]^{0.1} \left[O_2\right]^{1.65} \tag{5}$$
$$k_{2,f} = 2.64 \times 10^9 e^{-15097/T} \left[C_{10}H_{22}\right]^{0.25} \left[O_2\right]^{1.5} \tag{6}$$
$$k_{3,f} = 2.24 \times 10^{12} e^{-20129/T} \left[CO\right] \left[O_2\right]^{0.25} \left[H_2O\right]^{0.5} \tag{7}$$
$$k_{4,f} = 5.00 \times 10^8 e^{-20129/T} \left[CO_2\right] \tag{8}$$

IV. Results

A. Turbulent Spectrum

To assess the grid quality, the turbulent spectra is analyzed for each case. The results are shown in Figure 3. Both simulations show a turbulent spectrum that agrees with the expected $-5/3$ slope. This indicates that the current grid resolution is sufficient for the LES model used in this study. The point of analysis for each case is in the shear layer of an injector.

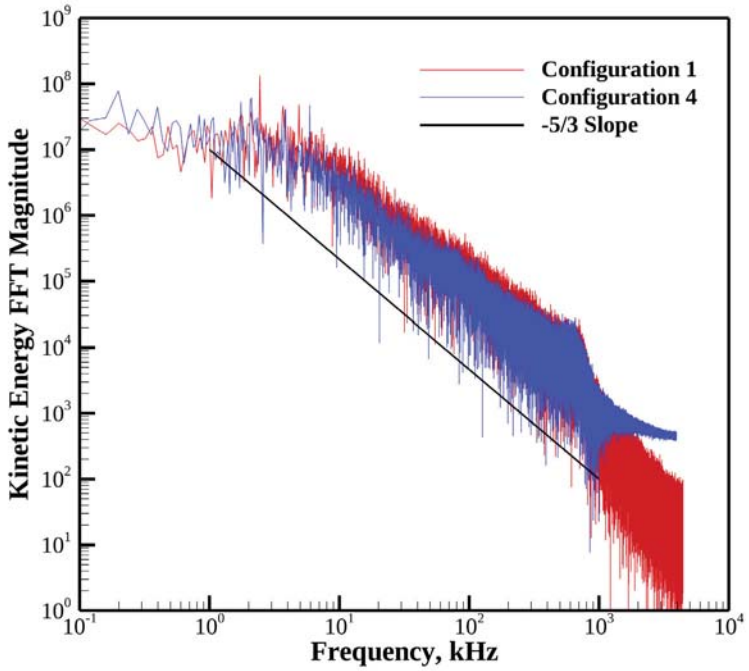

Figure 3: Turbulent spectrum for configuration 1 and 4.

B. Unsteady Pressure Signal

The unsteady pressure signals at the side wall for configuration 1 and 4 are shown in Figure 4. For the 1W mode the side wall is expected to show the greatest amplitude variations because it is at the location of the pressure anti-node. Two 10 ms windows of time are shown. Unlike the experimental results which exhibited large differences in amplitudes between the two configurations both of the simulations have similar amplitudes. Configuration 1 has a slightly larger amplitude but also shows more variability in the peak-to-peak amplitudes compared with configuration 4. Both simulations do show limit cycle behavior, there are no periods of instability growth or damping. This is unlike previous work by Shipley et al. which failed to produce limit cycle amplitude in an unstable configuration.[19] The center of the chamber is a pressure node for the 1W mode and a pressure anti-node for the 2W mode, Figure 5 shows the unsteady pressure at the center of the chamber. Here again the simulations predict similar amplitudes for each of the two configurations. The pressure amplitudes are significantly lower at the center of the chamber compared to the side wall which is to be expected for a 1W mode. Representative amplitudes at the side wall are on the order of 200 kPa while amplitudes at the center are less than 100 kPa peak-to-peak.

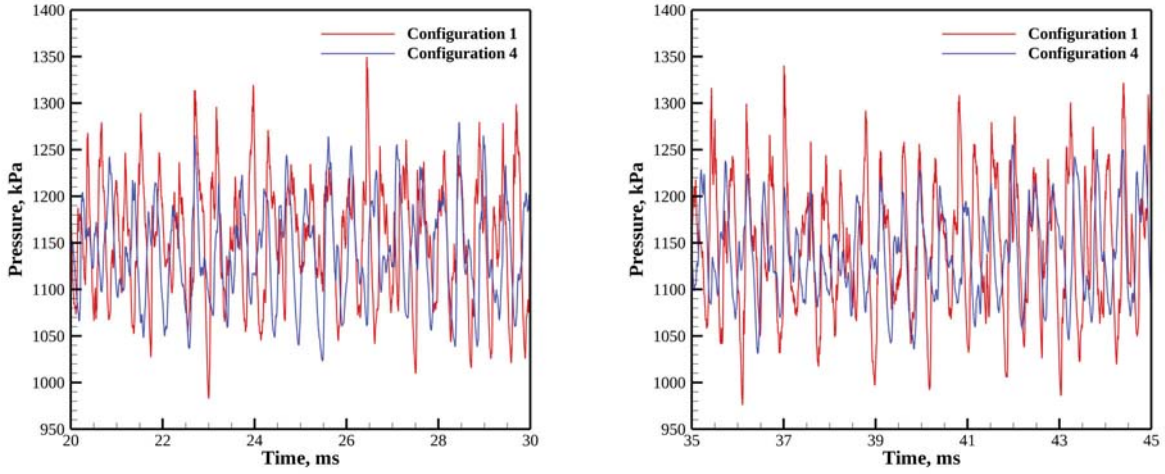

Figure 4: Unsteady pressure fluctuations on the right side of the chamber for configurations one and four. Two time instances are show which show consistent amplitudes between the two.

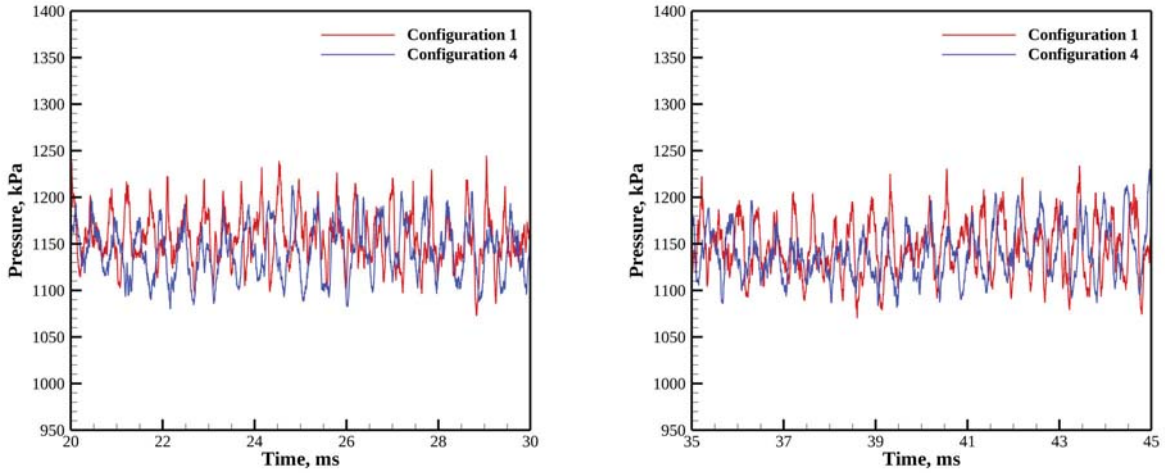

Figure 5: Unsteady pressure fluctuations at the center of the chamber for configurations one and four. Two time instances are show which show consistent amplitudes between the two.

C. Power Spectral Density Analysis

The unsteady pressure signals can be analyzed using a power spectral density (PSD) analysis to determine the spectral content of the signals. A total of 25 ms of data is used for analysis, covering the period between 20 ms and 45 ms. The unsteady pressure signal is converted to a uniformly spaced signal with a sample interval of 1×10^{-7} s. This results in a maximum frequency of 5000 kHz, well above the frequencies of interest for this study. The 25 ms of data used provides a frequency resolution of 40 Hz. PSD plots for each configuration at the side wall are shown in Figure 6. Configuration one shows a well-defined peak at 2440 Hz, above the experimentally reported frequency (see table 3). The second mode is not clearly defined and is bifurcated with peaks at 3400 Hz and 3680 Hz. Configuration four shows strong first and second peeks at 2080 Hz and 3840 Hz; modes above the second mode are not well resolved. A quantitative summary of the amplitudes and frequency, along with a comparison to the experiment is shown in Table 3. Both simulations have chamber pressures (p_c) larger than the experimental values. For configuration one the simulated frequency of the first mode is 400 Hz higher than the experiment. The amplitude is lower, 23% of the chamber pressure compared with 65%. The frequency prediction for Configuration 4 is better, 2080 Hz compared with 1855 Hz but is still on the higher side. This has been the case with prior single element studies and may be related to the adiabatic wall boundary conditions in the chamber.[10] Amplitude predictions are 12% of the chamber pressure compared with 8% observed in the experiment.

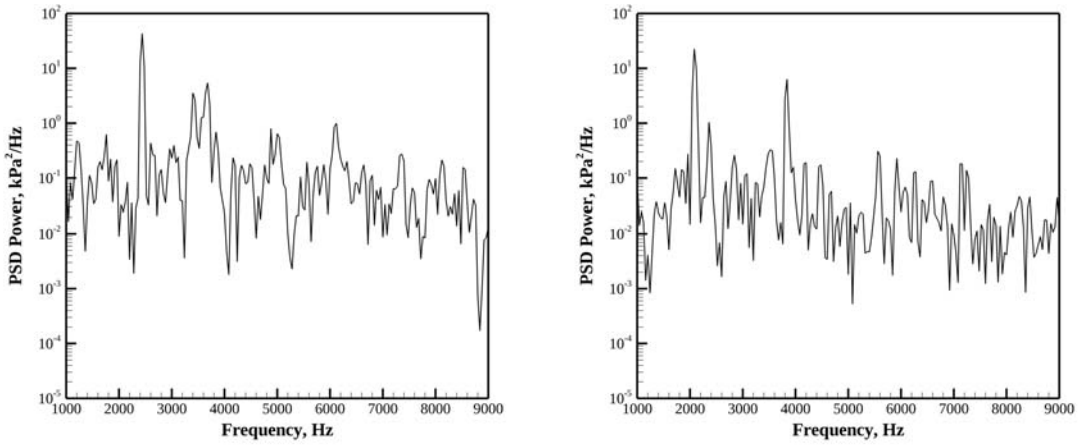

(a) Configuration 1

(b) Configuration 4

Figure 6: Power spectral density plots for configuration one and configuration four, in each case the signal at the side wall is used.

A PSD analysis was also completed at the center of the chamber, and inside the cup region of the center injector. The plots are shown in Figure 7. Configuration one shows strong peaks at 2440 Hz and 3680 Hz in both the chamber and the cup region. It is not expected to see significant activity at the 1W frequency in the center of the chamber. Configuration four has a dominate peak at 3840 Hz in both the chamber and the cup region, this is 300 Hz less than the expected 2W frequency (based on the 1W), but is same frequency that was identified at the side wall. For both configurations the response amplitudes in the injector are higher than those in the combustor, this indicates that the study element is being excited by the modes present in the combustor. The PSD shows that the study element in configuration one is responding to the dominate first mode frequency in the chamber, this is not the case for configuration four which only shows activity at the second mode which is to be expected. These results suggest that the excited mode in configuration one may not be a pure transverse mode, or the excited center element is altering it.

Table 3: Power spectral density results for the signal at the wall.

	Experiment	Simulation
Configuration 1		
1W Frequency, Hz	2032	2440
p', kPa	620	259
p_c, kPa	965	1148
p'/p_c	65%	23%
Configuration 4		
1W Frequency, Hz	1855	2080
p', kPa	70	139
p_c, kPa	815	1139
p'/p_c	8%	12%

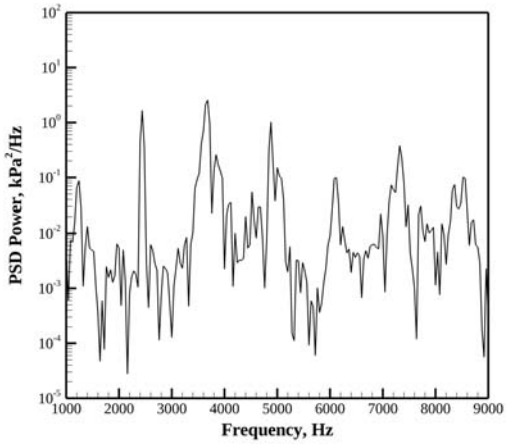

(a) Configuration 1, chamber

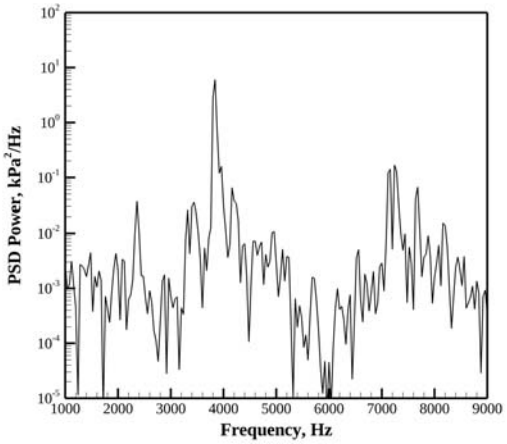

(b) Configuration 4, chamber

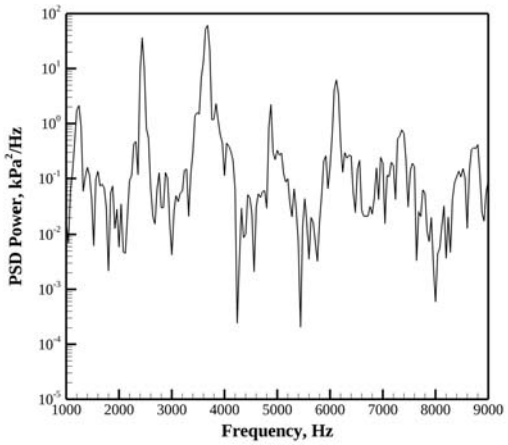

(c) Configuration 1, injector

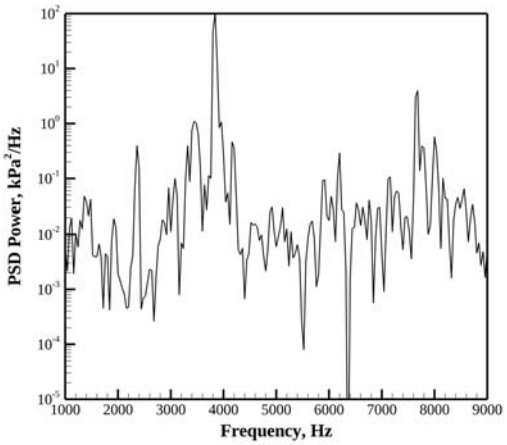

(d) Configuration 4, injector

Figure 7: Power spectral density plots for configuration one (left) and configuration four (right), the top row shows the spectrum in the chamber and the lower row shows the spectrum in the cup

D. Configuration 1 Flowfield

Figure 8 shows the pressure trace on the right side wall for the cycle of interest, numbered points indicate times of analysis in subsequent figures. Figure 9 shows the unsteady pressure in the combustor and injectors for the time 37.55 ms through 38.03 ms. The cycle does not show the expected transverse wave inside the combustor. There is some evidence of the pressure oscillating between high and low at the top of the combustor just below the injector plate, but this is highly localized. It is expected that the pressure wave would span the entire height of the combustor. There is evidence of excitation in the center element that was observed in the PSD plots. Frame 2 and 3 show low and high pressure near the cup region. The side elements are also excited. The wave in the center element is stronger than those present in side elements. The center element wave also appears to be more coherent compared to the driving elements. In a 1W transverse mode you would expect the pressure signals in the driving elements on opposite sides of the chamber to be 180˚ out-of-phase. This does not seem to be the case. Frame 6 shows low pressure near the cup region for all elements simultaneously. There is also substantial axial variation in the pressure field near the injector plate and in the second half of the nozzle, seen in frames 3, 6 and 9. This field plot along with the PSD data suggests that the excitation in configuration one is not a transverse mode, which could explain why the amplitude and frequency differ substantially from the experiment. The reason for not achieving a transverse mode is not known.

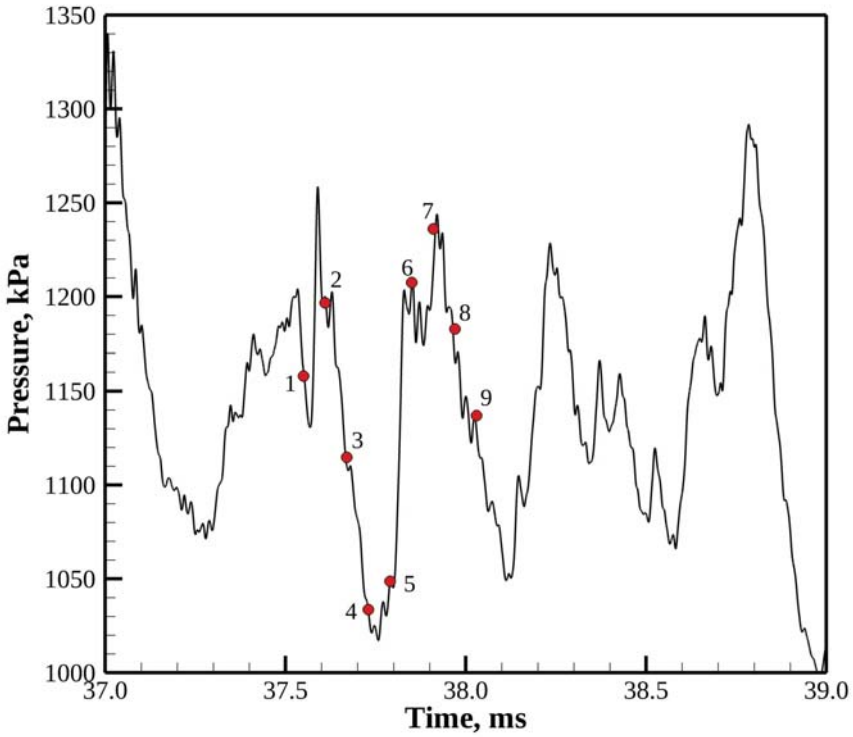

Figure 8: Pressure wave on the right wall, points of analysis are marked.

The temperature flowfield is shown for the time period in Figure 10. Similar to the pressure plots there is no evidence of a strong transverse instability. There is some unsteadiness in the vicinity of the injector plate, but with an unstable transverse mode it is expected to see large side to side shifts in the location of the oxidizer core as the wave passes by. This is not visible. The temperature field is also non-uniform; the region around the center element is significantly cooler than the sides of the combustor for all time instances.

Figures 11 and 12 look at the two driving injectors on the right side of the chamber. Figure 11 shows the mass fraction of RP1 as it is injected into the chamber and Figure 12 shows the corresponding fuel consumption rate. The fuel mass fraction shows significant penetration into the combustor, there are large

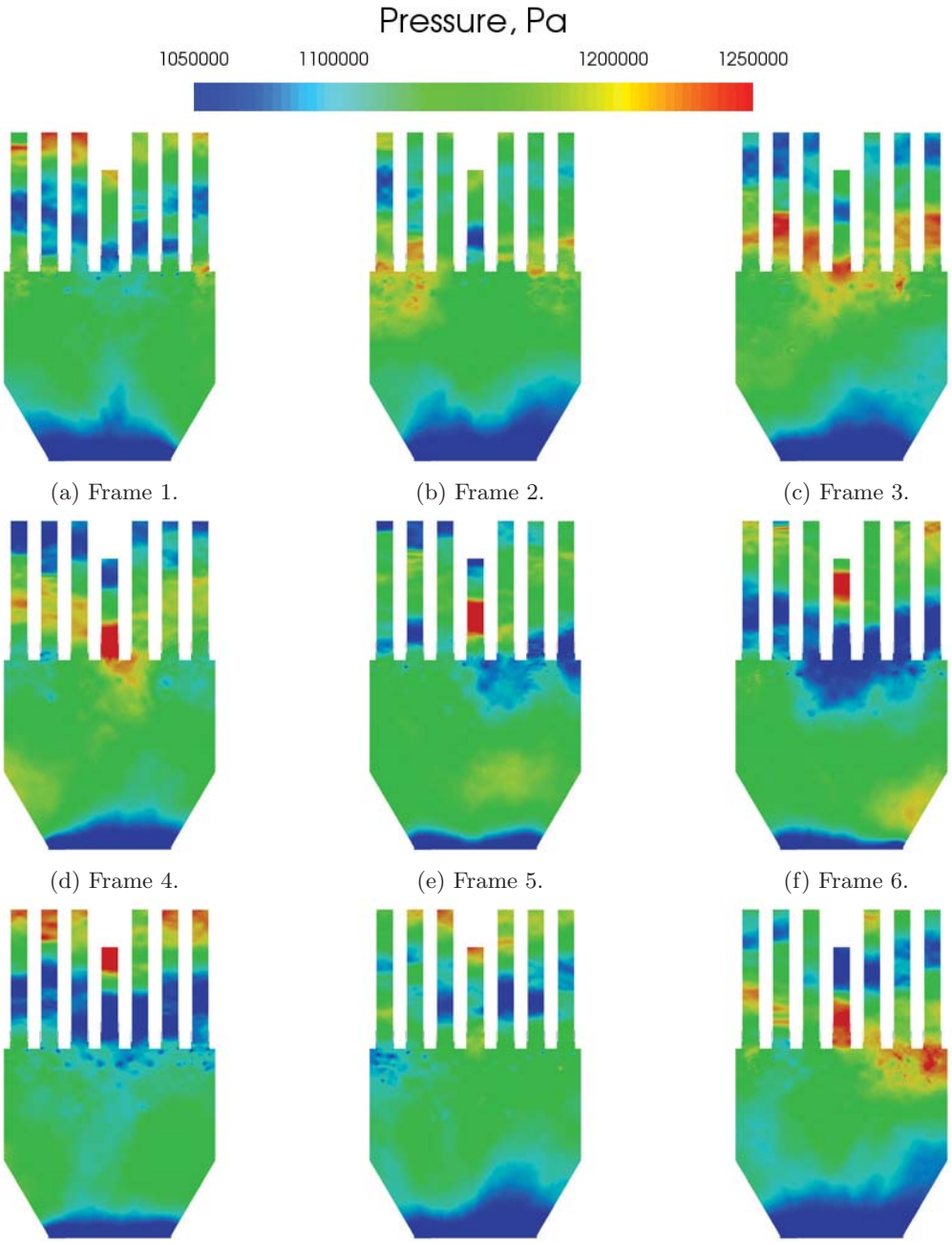

(a) Frame 1. (b) Frame 2. (c) Frame 3.

(d) Frame 4. (e) Frame 5. (f) Frame 6.

(g) Frame 7. (h) Frame 8. (i) Frame 9.

Figure 9: Pressure flowfield, a single cycle is shown; 0.48 ms total elapsed time, spaced 0.06 ms apart. Frame numbers corespond to the points identfied in Figure 8.

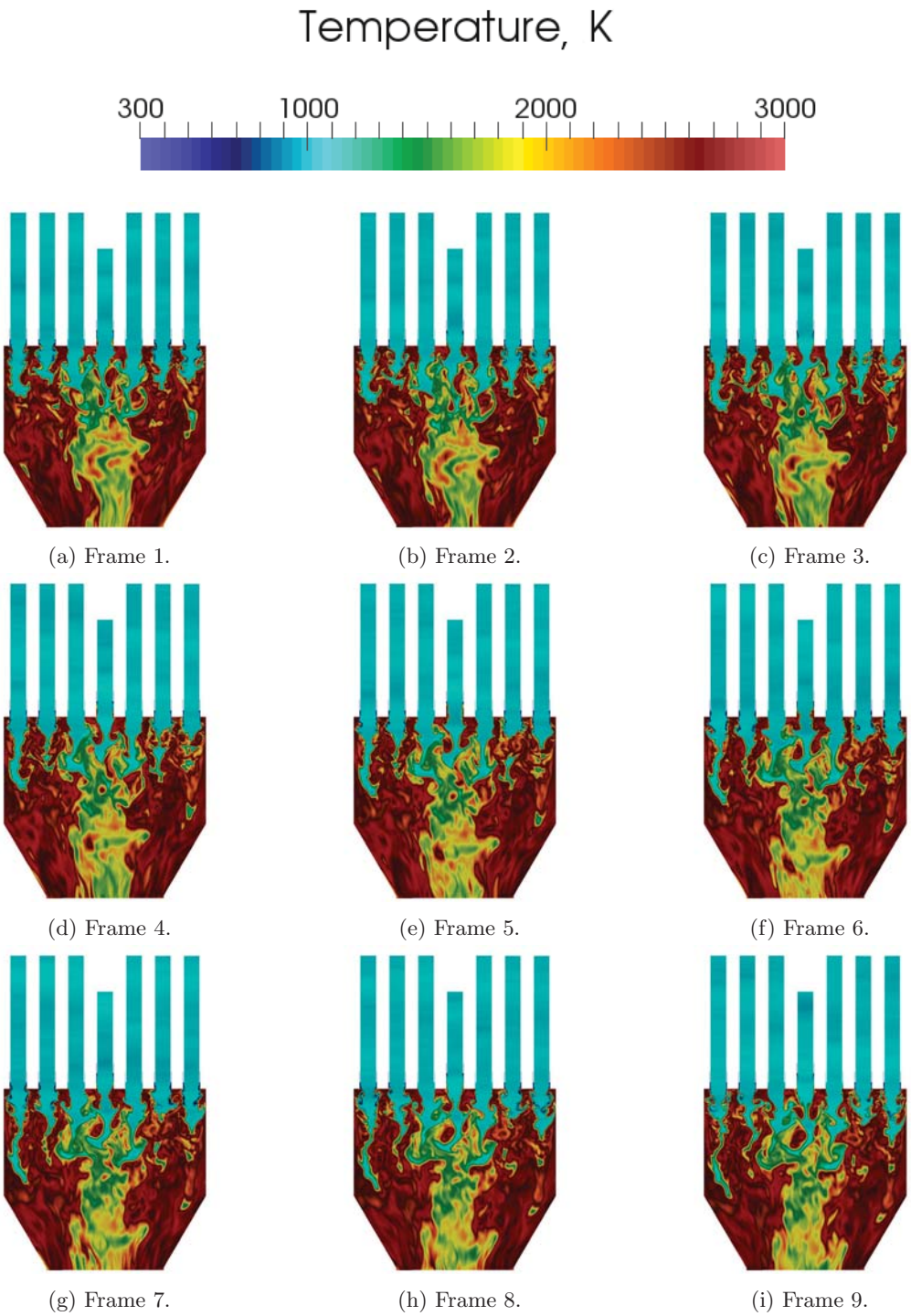

(a) Frame 1. (b) Frame 2. (c) Frame 3.

(d) Frame 4. (e) Frame 5. (f) Frame 6.

(g) Frame 7. (h) Frame 8. (i) Frame 9.

Figure 10: Temperature flowfield, a single cycle is shown; 0.48 ms total elapsed time, spaced 0.06 ms apart. Frame numbers corespond to the points identfied in Figure 8.

regions away from the injector with a fuel mass fraction larger than 0.25. In the region adjacent to the injector plate there is minimal evidence of the transverse instability. Frames 3, 4, and 9 of the mass fraction show the separation between the streams of fuel closing, this occurs during the high pressure portion of the cycle as the wave has passes through this injection region. The fuel consumption rate is amplified during this period, indicating a coupling between the pressure and combustion heat release. Compare the heat release at frame 5 with the heat release in frame 9. Frame 5 shows very little consumption of fuel, especially for the outermost injector, this is the low pressure point of the cycle. Frame 9, the high pressure point, shows a significant rate of fuel consumption for both injectors.

Prior studies by Shipley et al.[19] stated the importance of vortex impingement of the driving injector with each other as an amplification method. That phenomenon is not present in this case, possibly because the lower amplitude transverse wave does not bring the two vortices sufficiently close to each other. Unlike previous single element work there is virtually no fuel consumption in the cup region of the injector. There is also no evidence of significant periods of the fuel supply being cut off despite the presence of acoustic waves in the injectors. The driving injectors use RP1 while the previous studies used CH_4, it is possible that the higher molecular weight fuel is more resistant to the wave disrupting the fuel stream. It is also possible that the shorter cup region and the transition between a transverse wave in the combustor and a longitudinal wave in the injector do not render the same effect that a pure longitudinal wave does on an injector.

Figures 13 and 14 show the behavior near the study element in the center of the chamber. The mass fraction and consumption rate of C_2H_6 are shown. Compared with the driving elements the behavior of the study element is different. Virtually no regions of high concentrations fuel are present downstream of the injector. Fuel is shed from the corner of the injection plate and quickly consumed. There is evidence of fuel that is trapped in shed vortices, but it is quickly consumed. There is burning in the cup region and that hinders the fuel supply coming into the combustor. The is most obvious in frame 5. Notice the fuel pushed outward just past the injection point and the corresponding fuel consumption downstream in the cup region along the wall. This follows the high pressure in the cup region that was present in frame 4. Though not exactly the same this behavior is similar to the instability mechanism present in the CVRC experiment. In this case there is not a complete cut off of the fuel supply.

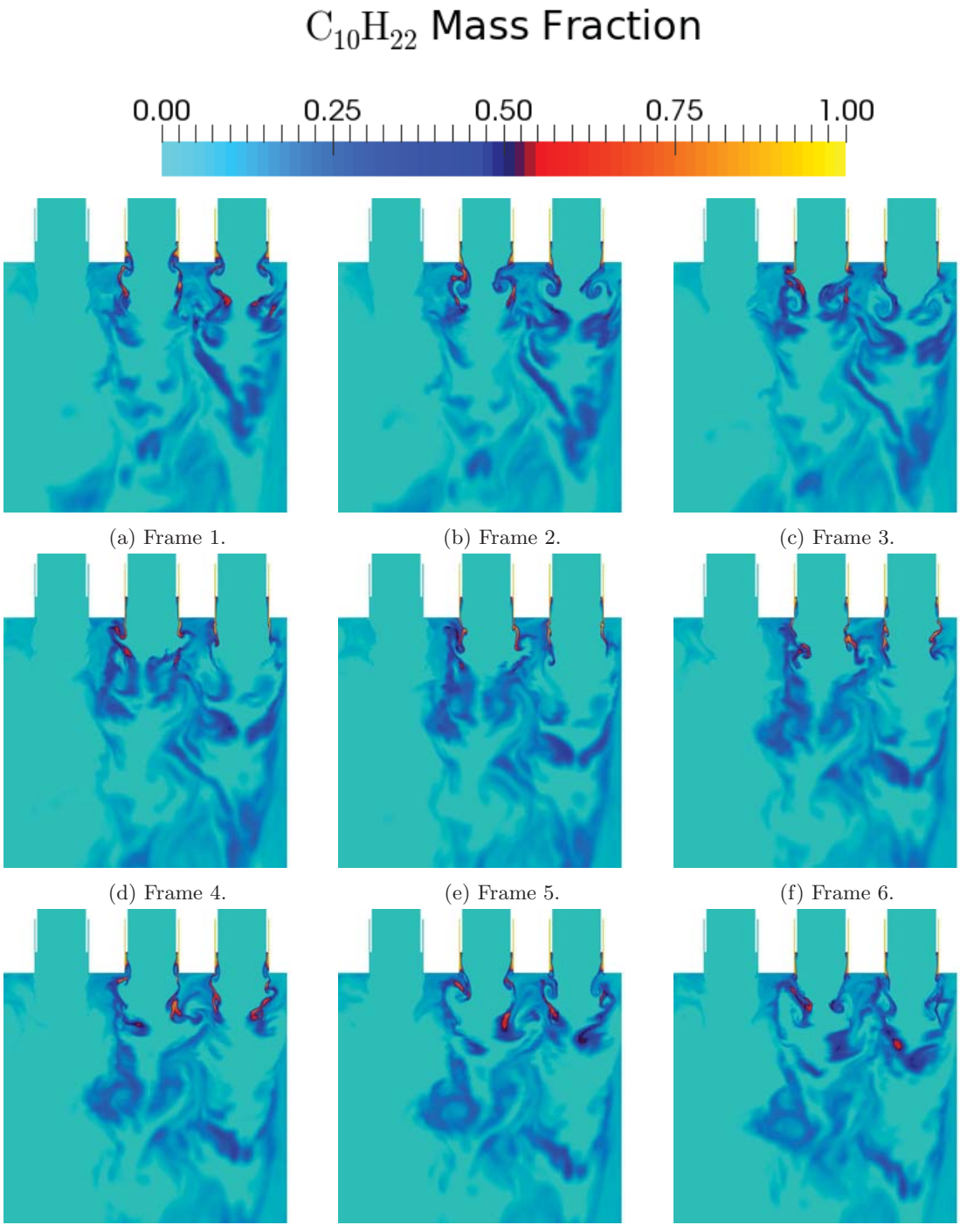

(a) Frame 1. (b) Frame 2. (c) Frame 3.

(d) Frame 4. (e) Frame 5. (f) Frame 6.

(g) Frame 7. (h) Frame 8. (i) Frame 9.

Figure 11: Mass fraction of RP1 near driving elements on the right side of the combustor. Frame numbers corespond to the points identfied in Figure 8.

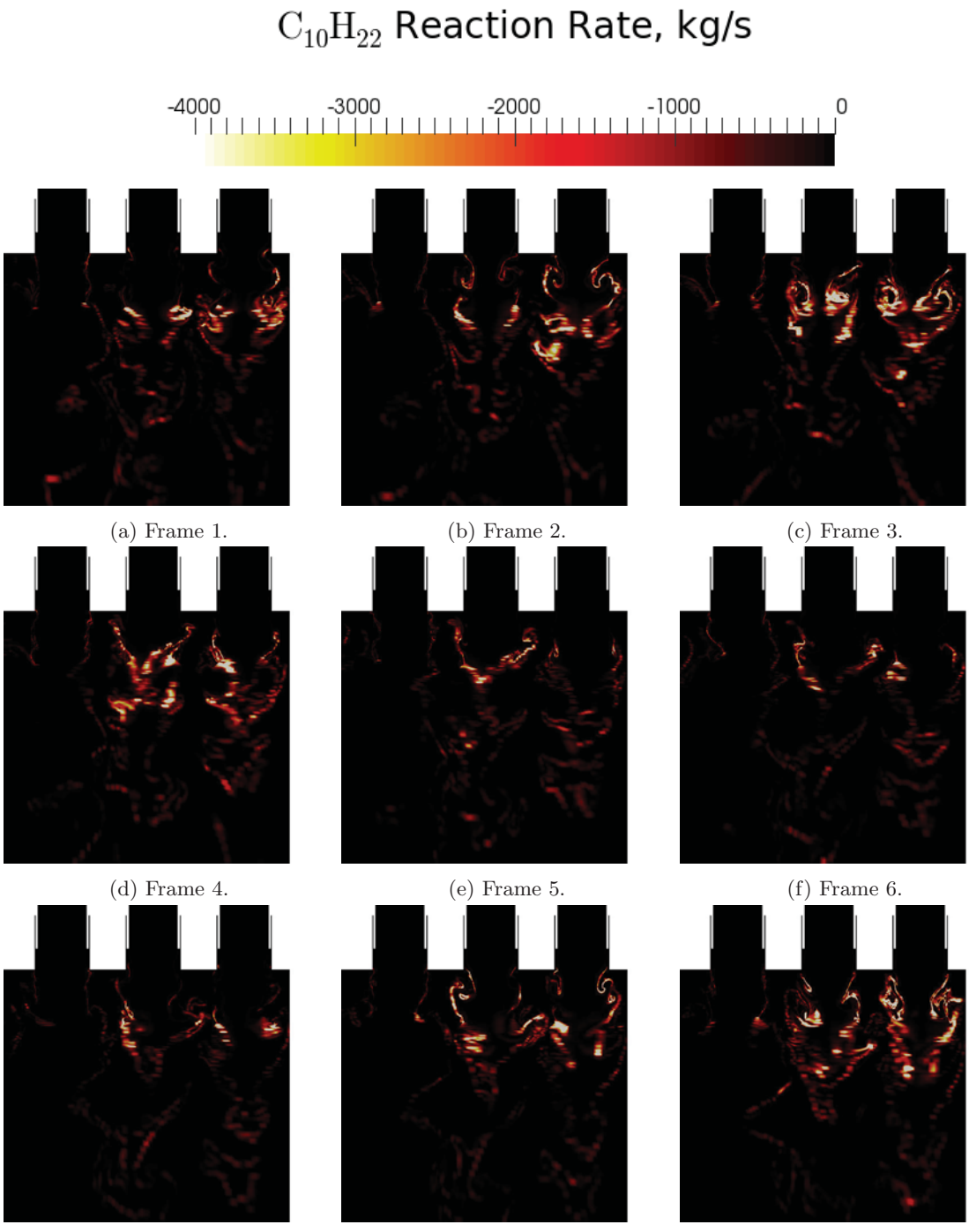

(a) Frame 1. (b) Frame 2. (c) Frame 3.

(d) Frame 4. (e) Frame 5. (f) Frame 6.

(g) Frame 7. (h) Frame 8. (i) Frame 9.

Figure 12: Consumption of RP1 near driving elements on the right side of the combustor. Frame numbers corespond to the points identfied in Figure 8.

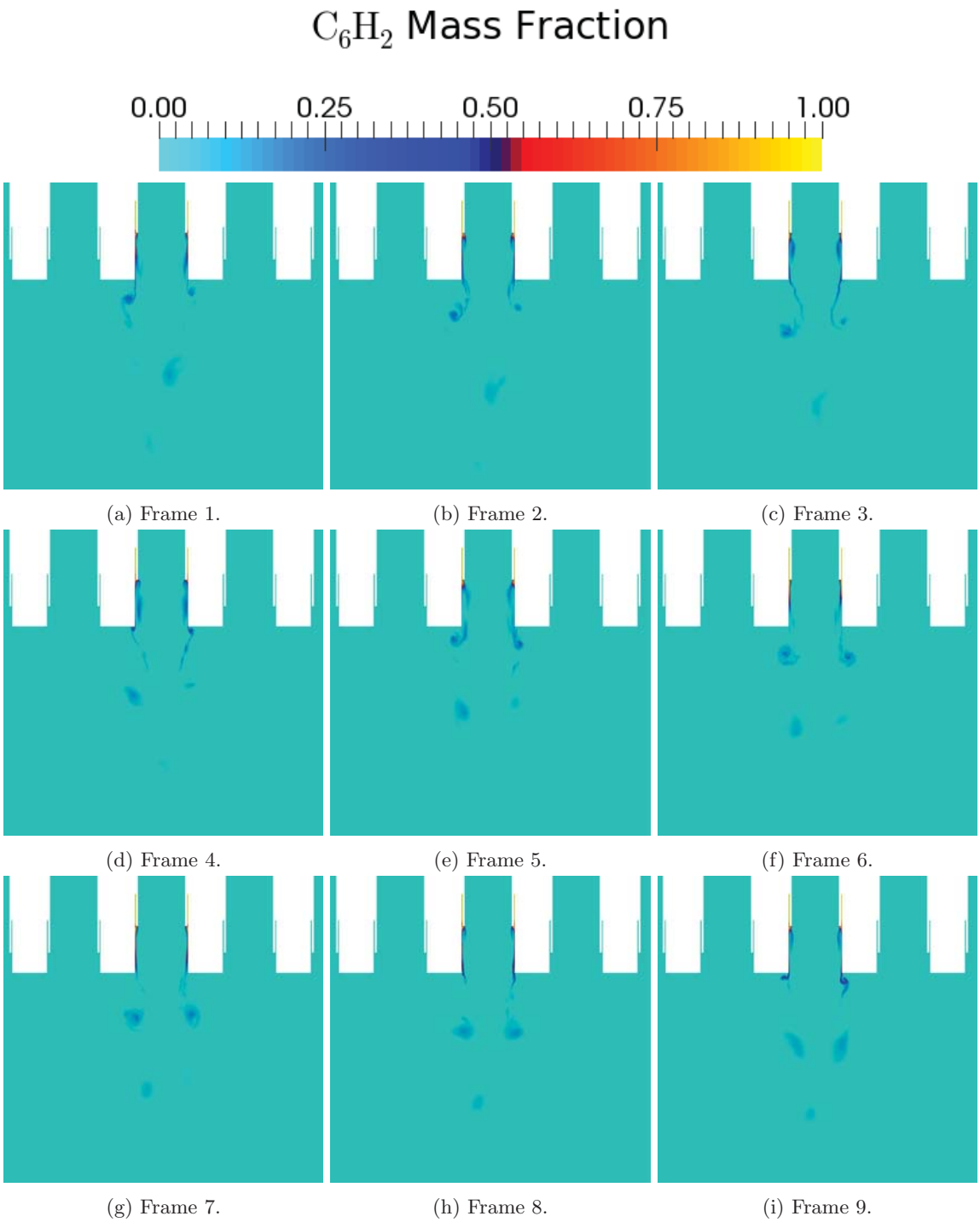

(a) Frame 1. (b) Frame 2. (c) Frame 3.

(d) Frame 4. (e) Frame 5. (f) Frame 6.

(g) Frame 7. (h) Frame 8. (i) Frame 9.

Figure 13: Mass fraction of C_2H_6 near the study element in the center of the combustor. Frame numbers corespond to the points identfied in Figure 8.

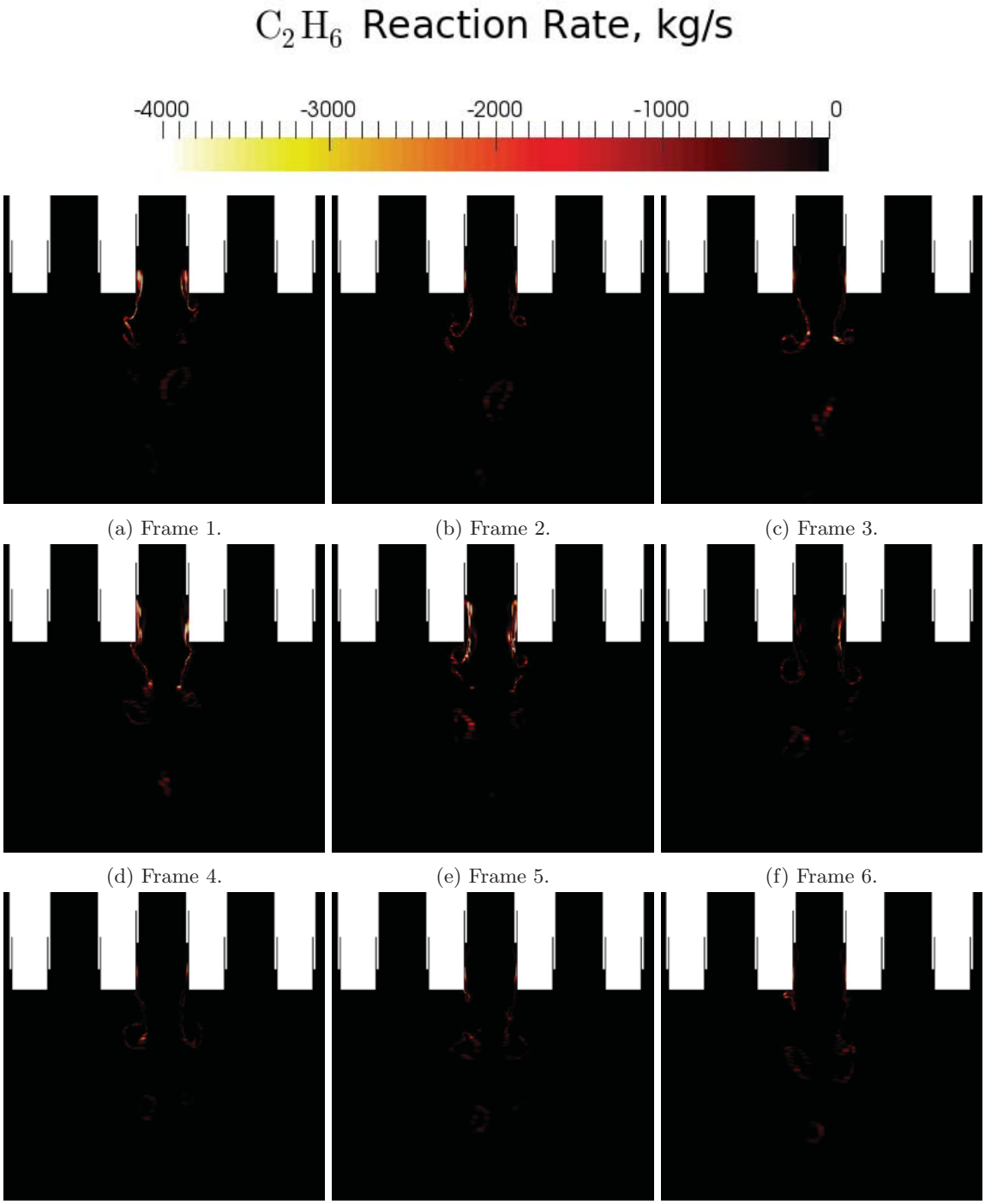

(a) Frame 1. (b) Frame 2. (c) Frame 3.

(d) Frame 4. (e) Frame 5. (f) Frame 6.

(g) Frame 7. (h) Frame 8. (i) Frame 9.

Figure 14: Consumption of C_2H_6 near the study element in the center of the combustor. Frame numbers corespond to the points identfied in Figure 8.

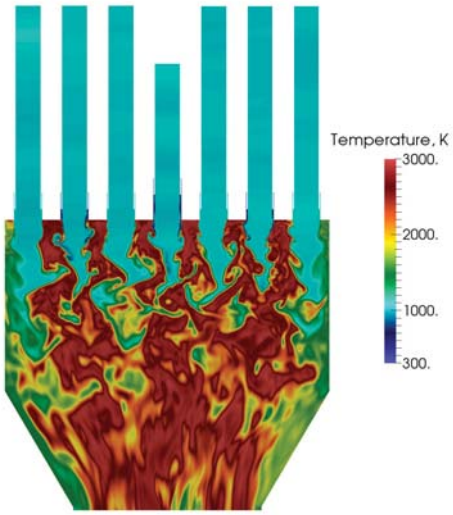

Figure 15: Temperature of configuration 4.

E. Configuration 4 Flowfield

The behavior of configuration 4 is different from configuration 1. In this case we see more of the expected results from a transverse instability wave. An example of the differences is shown in Figure 15, here a single frame of the temperature field is shown. Notice the difference in the center of the chamber compared to what was previously shown in Figure 10. There are significantly higher temperatures in the center of the chamber.

Figure 16 shows the pressure at the right side wall for a selected cycle. The cycle of interest is indicated and spans between 42.86 ms and 43.34 ms. The pressure field in the chamber is shown during this cycle in Figure 17, the points shown are those numbered 1-9 in Figure 16. The pressure clearly indicates a transverse mode in the combustor. At the start of the cycle the pressure is low, it reaches a maximum half way through the cycle (frame 4 and 5) and returns to a low pressure at the end of the cycle (frame 9). The right side of the chamber is 180° out-of-phase with the left side which is to be expected. Acoustic modes are present in the injectors. The pressure wave in the study element is operating at approximately twice the frequency of the chamber, it shows a low pressure at the start, middle, and end of the cycle in the cup region. This again is consistent with what is to be expected for a transverse mode. Unlike configuration one the transverse pressure wave is occurring throughout the entire length of the combustor. There is also less axial variation in the pressure compared with configuration one.

Figures 18 and 19 show the fuel injection of driving element located on the right side of the chamber. Note that in this case only one element is flowing fuel. There is significantly less fuel present here compared to configuration one, this is because only one driving element is flowing fuel. The penetration length of high concentration fuel is still large compared to prior single element studies. The flowfield shows evidences of the interaction between the transverse wave and the injected fuel present inside the combustor. Unlike the first configuration which looked more or less the same at each time instance here we see distinct differences. When the pressure on the right side is lower there are regions of high concentration fuel (mass fraction larger than 0.5) in the combustor, this is seen in frames 4-6. As the pressure increases these regions become less pronounced. The fuel consumption shows no burning in the cup region, and a flame which is lifted from the injector plate. The region of fuel consumption is in the shear region closer to the injector and moves to the center of the element further away. As the pressure increases (frames 7-9) there is a marked increase in the magnitude of the fuel consumption rate. This is also the time when combustion is also present outside of the shear region. This is because the transverse wave that passed through pushes the fuel stream away from the shear layer. Frame 9 is an example of this, here the pressure wave has just moved from left to right, the fuel consumption rate and mass fraction show a shift in that direction.

Figures 20 and 21 show the behavior of the study element in the center of the chamber. Compared to the driving element the fuel is present in the chamber with higher concentrations, especially in the shear layer

region just downstream of the injection plate. There are high concentrations of fuel along the cup region wall at all times. Vortices with high concentrations of fuel are shed from the study element and propagate downstream where they eventually burn. The flame is detached and there is no fuel consumption in the cup region, another difference from configuration one. Significantly more fuel is present in the combustor compared to configuration one and there is no evidence of fuel any fuel supply disruptions. The mass fraction plots show the influence of the transverse wave as the shear layer is shifted and not parallel to the center line. The heat release is also similar at all times despite the presence of the transverse wave. There does not appear to be a strong coupling in this case between the chamber acoustics and the combustion from the study element.

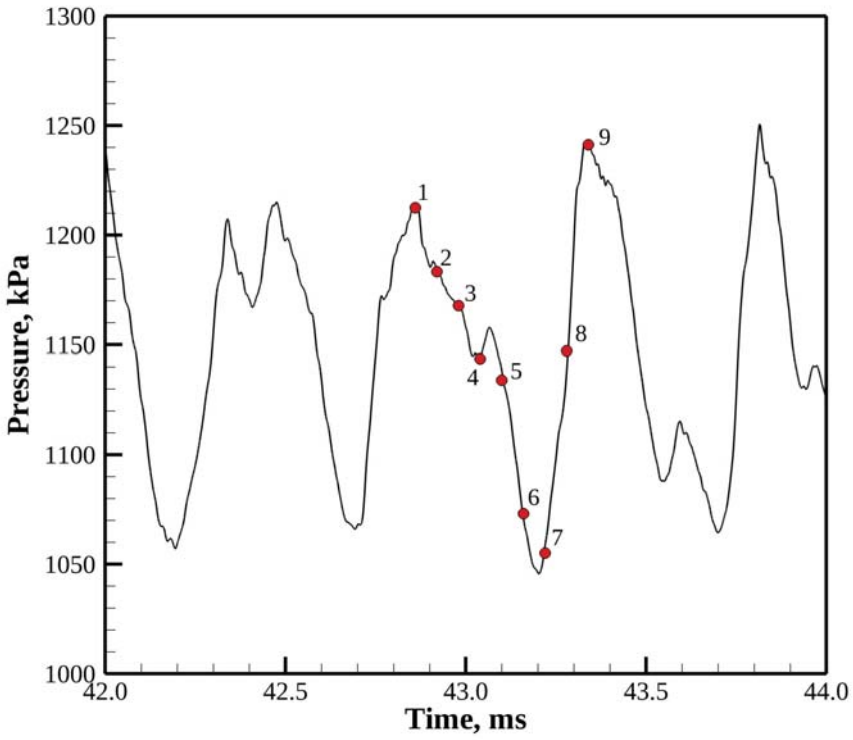

Figure 16: Pressure wave on the right wall, points of analysis are marked.

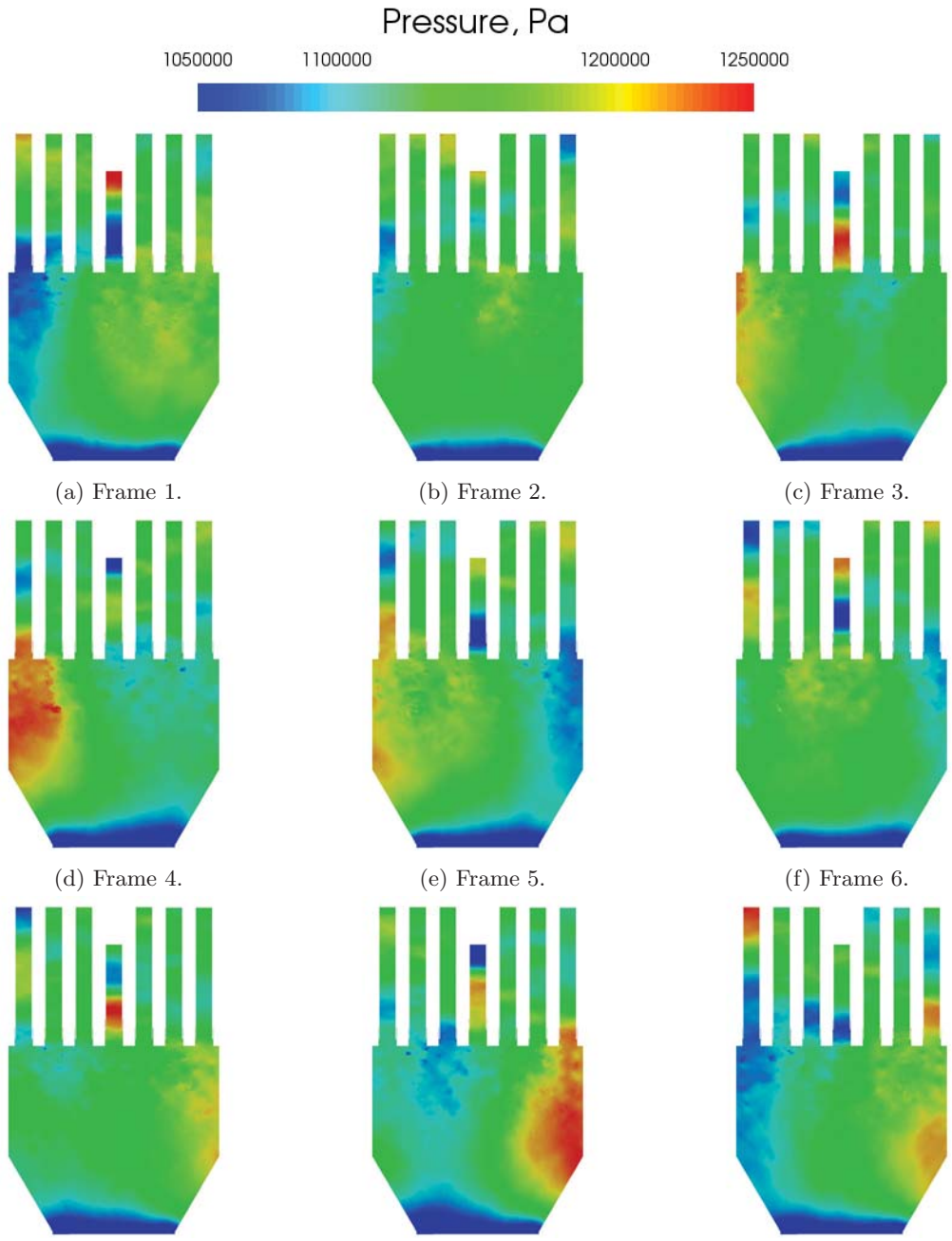

(a) Frame 1. (b) Frame 2. (c) Frame 3.

(d) Frame 4. (e) Frame 5. (f) Frame 6.

(g) Frame 7. (h) Frame 8. (i) Frame 9.

Figure 17: Pressure Flowfield, a single cycle is shown; 0.48 ms total elapsed time, spaced 0.06 ms apart. Frame numbers corespond to the points identfied in Figure 16.

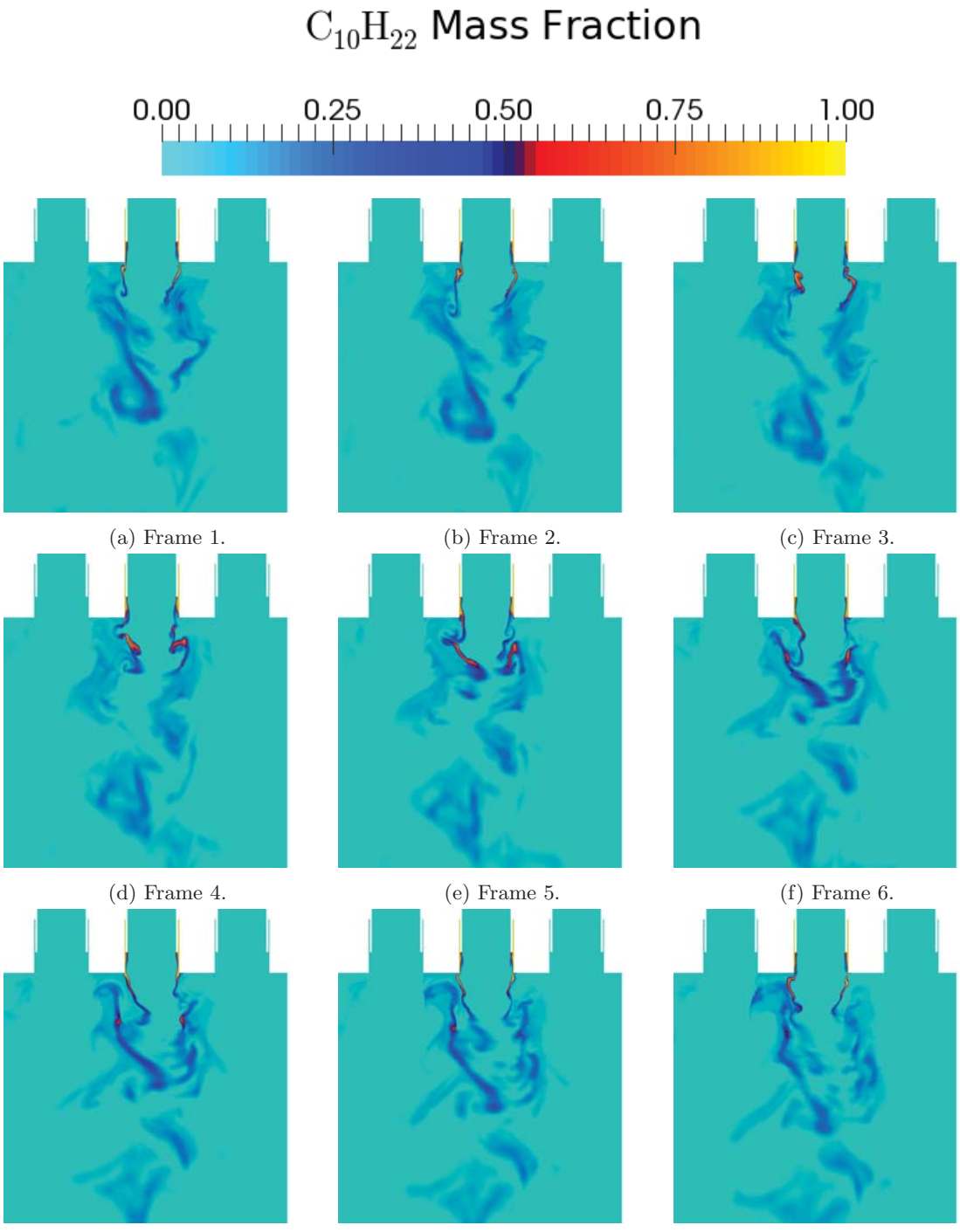

(a) Frame 1. (b) Frame 2. (c) Frame 3.

(d) Frame 4. (e) Frame 5. (f) Frame 6.

(g) Frame 7. (h) Frame 8. (i) Frame 9.

Figure 18: Mass fraction of RP1 near driving elements on the right side of the combustor. Frame numbers corespond to the points identfied in Figure 16.

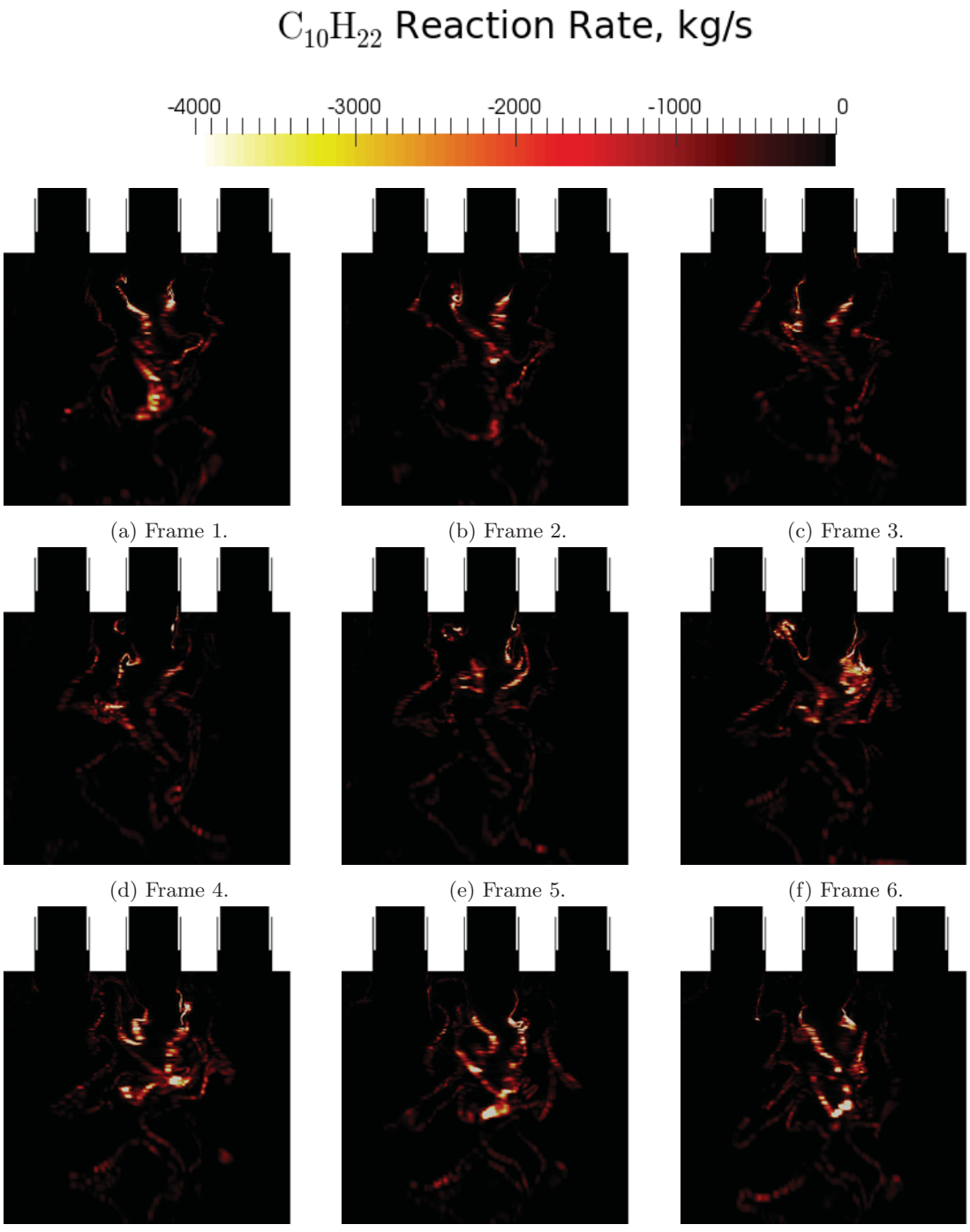

(a) Frame 1. (b) Frame 2. (c) Frame 3.

(d) Frame 4. (e) Frame 5. (f) Frame 6.

(g) Frame 7. (h) Frame 8. (i) Frame 9.

Figure 19: Consumption of RP1 near driving elements on the right side of the combustor. Frame numbers corespond to the points identfied in Figure 16.

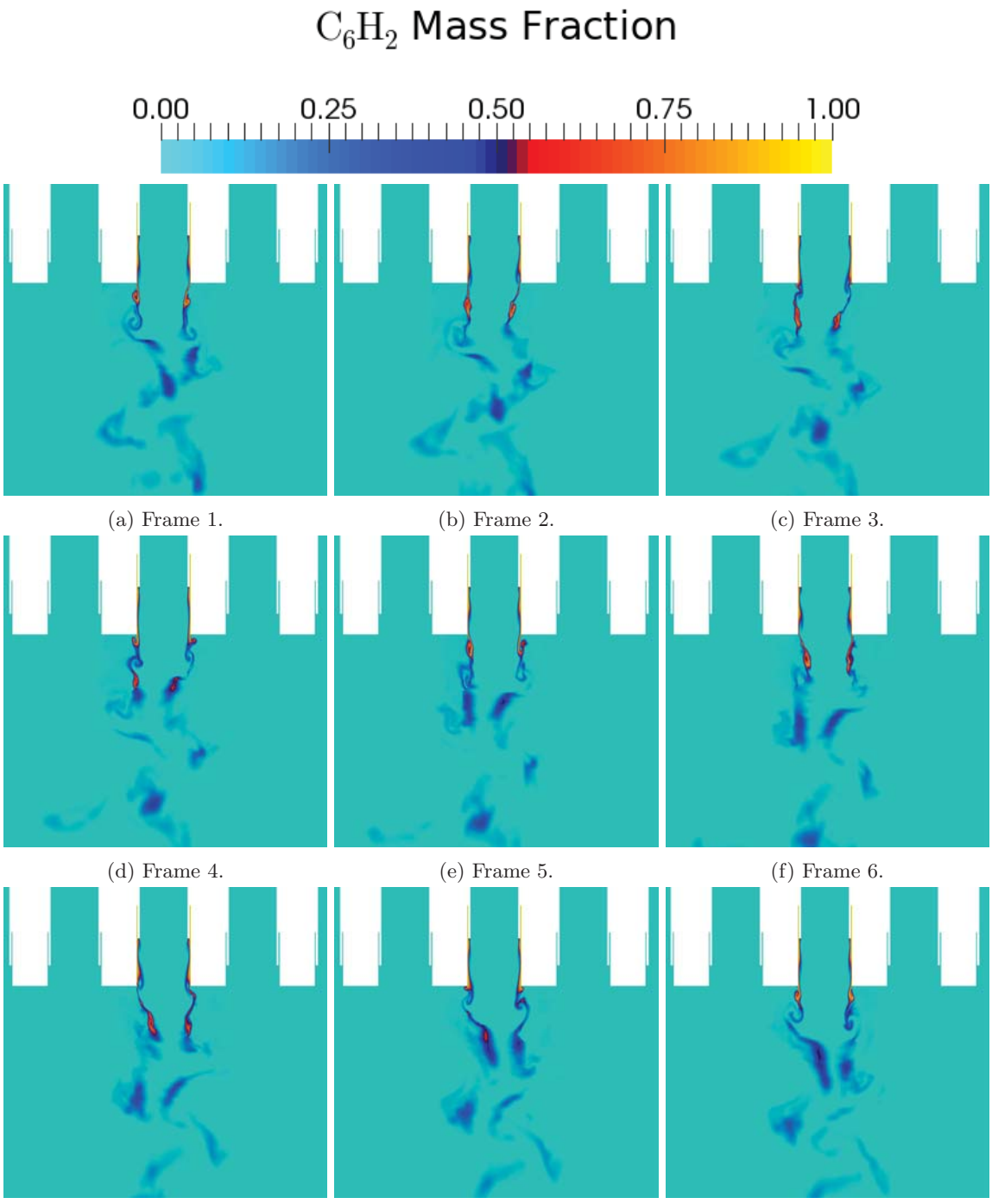

(a) Frame 1. (b) Frame 2. (c) Frame 3.

(d) Frame 4. (e) Frame 5. (f) Frame 6.

(g) Frame 7. (h) Frame 8. (i) Frame 9.

Figure 20: Mass fraction of C_2H_6 near the study element in the center of the combustor. Frame numbers corespond to the points identfied in Figure 16.

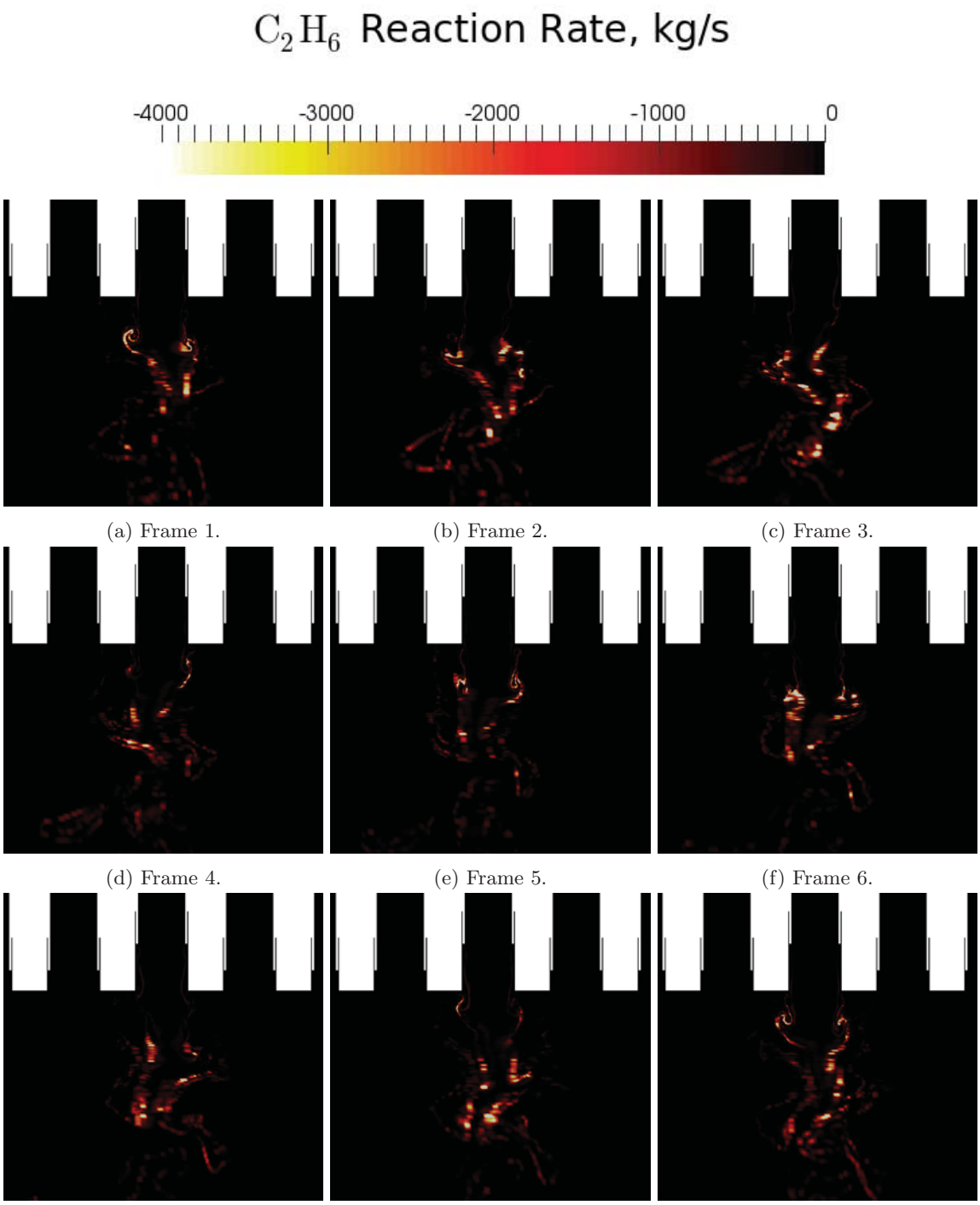

(a) Frame 1. (b) Frame 2. (c) Frame 3.

(d) Frame 4. (e) Frame 5. (f) Frame 6.

(g) Frame 7. (h) Frame 8. (i) Frame 9.

Figure 21: Consumption of C_2H_6 near the study element in the center of the combustor. Frame numbers corespond to the points identfied in Figure 16.

F. Time Averaged Comparison

As a final comparison between the two cases the time averaged temperature field is examined, it is shown in Figure 22. The flowfield for configuration one shows a significant decrease in the temperature downstream of the center injector. Configuration four does not show this. This may partially explain the higher than expected frequency. If a high amplitude transverse wave had been present more mixing between the cool center and hot side regions would have taken place, lowering the overall temperature which would reduce the frequency. The low temperature regions on the side of the combustor in configuration four are to be expected because the outermost injectors are flowing only oxidizer. From this figure it is clear that the combustion taking place from the study element is very different in each case. Experimentally there have been configurations where a change to the study element stabilized the flowfield. That was not done experimentally for this case but it may be what is happening in the simulation. It will be important to further determine the source of this in future work.

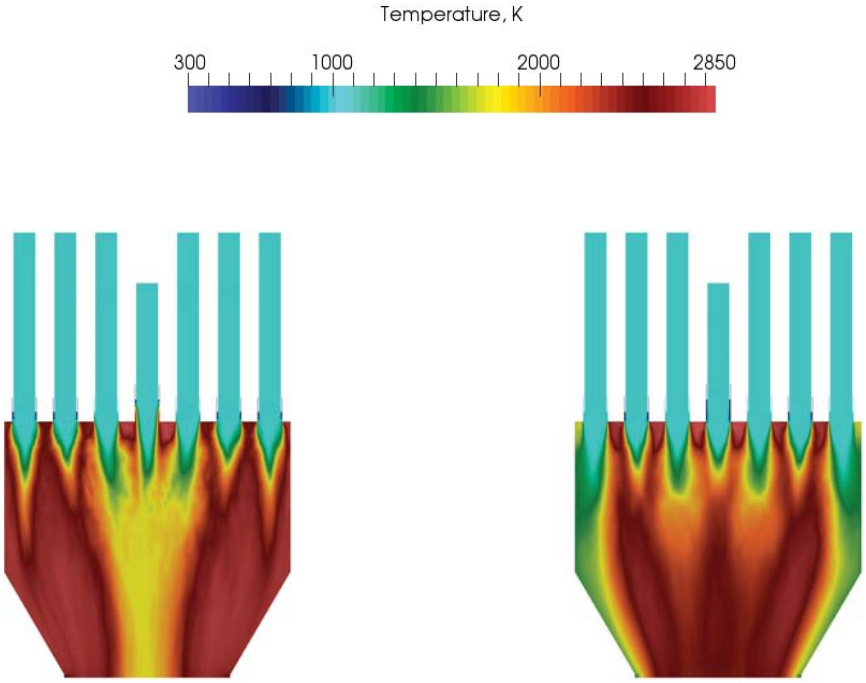

(a) Configuration 1 (b) Configuration 4

Figure 22: Time averaged temperature flowfield for each of the configruations.

V. Conclusions

Two configurations of the TIC were analyzed using reacting flow LES. The first configuration was experimentally unstable. The simulation for this configuration predicted amplitudes significantly lower than expected. Further examination of the spectral content showed results inconsistent with the expected transverse behavior. This was confirmed looking at the flowfield which showed a weak transverse mode and an excited center element. A second configuration which had lower amplitudes experimentally was also examined. Amplitude predictions showed higher than expected amplitudes by a factor of two. The amplitude was still lower than configuration one, which is consistent with the experiment. Unlike the first configuration this case showed the expected transverse behavior in the flowfield and spectral content of the pressure data.

The injectors, both driving and steady, in the second configuration showed shed vortices with fuel trapped in them. Fuel consumption occurred away from injector inside the combustor. In the case of the study element fuel consumption occurred further away from the injector plate compared with the driving injectors. The driving injectors showed evidence of coupling with the acoustics through amplification of the fuel con-

sumption. The observed instability mechanism in the single element longitudinal studies was not present in the driving elements for either configuration or the study element of configuration four. Some evidence of burning in the cup and partial fuel supply cutoff was observed in the study injector of configuration one. All of the injectors had combustion occurring throughout the cycles, unlike the single element studies which showed very clear periods of minimal heat release during a cycle. The current simulations do improve on the prior seven element simulation in terms of reaching a limit cycle; the prior simulations were not able to achieve limit cycle behavior.

There are several additional steps to be taken to investigate why the current results are not a better match to the experimental data. It is possible that there is insufficient grid resolution, the grid size was 15.63 M cells, prior single element studies used 5 M cells, and thus it may be necessary to approach a resolution consistent with the single element studies for each injector. The RP fuel was modeled with a surrogate that has a molecular weight which is less than the actual RP used, and was treated as an ideal gas. Switching to a cubic equation of state and used a surrogate with a molecular weight which better approximates the actual fuel will both improve the density predictions and yield the correct injection velocities. Both of these items will be considered in future studies. The apparent stabilization effect that the study element had on configuration one must further be examined and better understood, either through additional simulations or data analysis, possible investigating experimental conditions where this was the case.

Acknowledgments

Computing resources were provided by the DoD High Performance Computing Modernization Program.

References

[1]Harrje, D. and Reardon, F., "Liquid Propellant Rocket Combustion Instability," Tech. Rep. SP-194, NASA, 1972.

[2]Oefelein, J. and Yang, V., "Comprehensive review of liquid-propellant combustion instabilities in F-1 engines," *Journal of Propulsion and Power*, Vol. 9, No. 5, 1993, pp. 657–677.

[3]Smith, R., Xia, G., Anderson, W., and Merkle, C., "Computational Studies of the effects of oxidiser injector length on combustion instability," *Combustion Theory and Modelling*, Vol. 16, No. 2, 2012, pp. 341–368.

[4]Srinivasan, S., Ranjan, R., and Menon, S., "Flame Dynamics During Combustion Instability in a High-Pressure, Shear-Coaxial Injector Combustor," *Flow Turbulence and Combustion*, Vol. Advanced Online Publication, 2014.

[5]Garby, R., Selle, L., and Poinsot, T., "Large-Eddy Simulation of Combustion Instabilities in a Variable-length Combustor," *Comptes Rendus Mécanique*, Vol. 341, No. 1-2, 2013, pp. 220–229.

[6]Harvazinski, M., Anderson, W., and Merkle, C., "Analysis of Self-Excited Combustion Instability using Two- and Three-Dimensional Simulations," *Journal of Propulsion and Power*, Vol. 29, No. 2, 2013, pp. 396–409.

[7]Feldman, T., Harvazinski, M., Merkle, C., and Anderson, W., "Comparison Between Simulation and Measurement of Self-Excited Combustion Instability," *48th AIAA/ASME/SAE/ASEE Joint Propulsion Conference and Exhibit*, AIAA, Atlanta, GA, July 2012, pp. 1–8.

[8]Tucker, P., Menon, S., Merkle, C., Oefelein, J., and Yang, V., "Validation of High-fidelity CFD simulations for rocket injector Designs," *44th AIAA/ASME/SAE/ASEE Joint Propulsion Conference and Exhibit*, AIAA, Hartford, CT, July 2008, pp. 1–20.

[9]Selle, L., Blouquin, R., Théron, M., Dorey, L., Schmid, M., and Anderson, W., "Prediction and Analysis of Combustion Instabilities in a Model Rocket Engine," *Journal of Propulsion and Power*, Vol. 30, No. 4, 2014, pp. 978–990.

[10]Harvazinski, M., Huang, C., Sankaran, V., Feldman, T., Anderson, W., Merkle, C., and Talley, D., "Coupling between hydrodynamics, acoustics, and heat release in a self-excited unstable combustor," *Physics of Fluids*, Vol. 27, 2015, pp. 45102.

[11]Muss, J., Nguyen, T., and Johnson, C., "User's manual for rocket combustor interactive design (ROCCID) and analysis computer program. Volume 1: User's manual," Tech. Rep. NASA-CR-187109, NASA, 1991.

[12]Muss, J., Nguyen, T., and Johnson, C., "User's manual for rocket combustor interactive design (ROCCID) and analysis computer program. Volume 2: Appendixes A-K," Tech. Rep. NASA-CR-187110, NASA, 1991.

[13]Yu, Y., Sisco, J., Rosen, S., Madhav, A., and Anderson, W., "Spontaneous Longitudinal Combustion Instability in a Continuously-Variable Resonance Combustor," *Journal of Propulsion and Power*, Vol. 28, No. 5, 2012, pp. 876–887.

[14]Morgan, C., *Response of a gas-gas shear coaxial injector to transverse instability*, Masters thesis, Purdue University, West Lafayette, IN, 2012.

[15]Pomeroy, B., *Measurement and analysis of combustion response to transverse combustion instability*, Ph.d. thesis, Purdue University, West Lafayette, IN, 2012.

[16]Pomeroy, B. and Anderson, W., "Transverse Instability Studies in a Subscale Chamber," *Journal of Propulsion and Power*, Vol. Article in Advance, 2016, pp. 1–9.

[17]Morgan, C., Shipley, K., and Anderson, W., "Comparative Evaluation Between Experiment and Simulation for a Transverse Instability," *Journal of Propulsion and Power*, Vol. 31, No. 6, 2015, pp. 1696–1706.

[18]Tudisco, P., Ranjan, R., and Menon, S., "Numerical Investigation of Transverse Forcing in a Multi-Element, Shear-

Coaxial, High Pressure Combustor," *54th AIAA Aerospace Sciences Meeting*, AIAA 2016-2155, San Diego, CA, January 2016, pp. 1–14.

[19]Shipley, K., Anderson, W., Harvazinski, M., and Sankaran, V., "A Computational Study of Transverse Combustion Instability Mechanisms," *50th AIAA/ASME/SAE/ASEE Joint Propulsion Conference, Propulsion and Energy Forum,*, AIAA 2014-3680, Cleveland, OH, July 2014, pp. 1–14.

[20]Popov, P. and Sirignano, W., "Transverse Combustion Instability in a Rectangular Rocket Motor," *Journal of Propulsion and Power*, Vol. 32, No. 3, 2016, pp. 620–627.

[21]Harvazinski, M., Talley, D., and Sankaran, V., "Influence of Boundary Condition Treatment on Longitudinal-Mode Combustion Instability Predictions," *Journal of Propulsion and Power*, Vol. 32, 2016, pp. 529–532.

[22]Kim, W., Menon, S., and Mongia, H., "Large Eddy Simulation of Gas Turbine Combustor Flow," *Combustion Science and Technology*, Vol. 143, 1999, pp. 25–62.

[23]Génin, F. and Menon, S., "Simulation of Turbulent Mixing Behind a Strut Injector in Supersonic Flow," *AIAA Journal*, Vol. 48, 2010, pp. 526–539.

[24]Génin, F. and Menon, S., "Studies of shock/turbulent Shear Layer Interaction Using Large-eddy Simulation," *Computers and Fluids*, Vol. 39, 2010, pp. 800–819.

[25]Masquelet, M. and Menon, S., "Large Eddy Simulation of Flame-Turbulence Interactions in a Shear Coaxial Injector," *Journal of Propulsion and Power*, Vol. 26, 2010, pp. 924–935.

[26]Génin, F. and Menon, S., "Dynamics of Sonic Jet Injection into Supersonic Crossflow," *Journal of Turbulence*, Vol. 11, 2010, pp. 1–30.

[27]Kim, W. and Menon, S., "An unsteady Incompressible Navier-Stokes Solver For Large Eddy Simulation of Turbulent Flows," *International Journal of Numerical Methods in Fluids*, Vol. 31, 1999, pp. 983–1017.

[28]Westbrook, C. and Dryer, F., "Chemical Kinetic Modeling of Hydrocarbon Combustion," *Progress in Energy and Combustion Science*, Vol. 1, No. 1, 1984, pp. 1–57.

[29]Harvazinski, M., Talley, D., and Sankaran, V., "Application of Detailed Chemical Kinetics to Combustion Instability Modeling," *54th AIAA Aerospace Sciences Meeting*, AIAA 2016-1931, San Diego, CA, January 2016, pp. 1–16.